Chemical Science

ROYAL SOCIETY OF CHEMISTRY

EDGE ARTICLE

View Article Online
View Journal | View Issue

Cite this: *Chem. Sci.*, 2023, **14**, 12676

All publication charges for this article have been paid for by the Royal Society of Chemistry

Nickel-catalysed asymmetric hydromonofluoromethylation of 1,3-enynes for enantioselective construction of monofluoromethyl-tethered chiral allenes†

Ying Zhang,‡[a] Jimin Yang,‡[b] Yu-Long Ruan,‡[a] Ling Liao,[a] Chuang Ma,[a] Xiao-Song Xue *[bd] and Jin-Sheng Yu *[ac]

Received 25th August 2023
Accepted 22nd October 2023

DOI: 10.1039/d3sc04474b

rsc.li/chemical-science

An unprecedented nickel-catalysed enantioselective hydromonofluoromethylation of 1,3-enynes is developed, allowing the diverse access to monofluoromethyl-tethered axially chiral allenes, including the challenging deuterated monofluoromethyl (CD_2F)-tethered ones that are otherwise inaccessible. It represents the first asymmetric 1,4-hydrofunctionalization of 1,3-enynes using low-cost asymmetric nickel catalysis, thus opening a new avenue for the activation of 1,3-enynes in reaction development. The utility is further verified by its broad substrate scope, good functionality tolerance, mild conditions, and diversified product elaborations toward other valuable fluorinated structures. Mechanistic experiments and DFT calculations provide insights into the reaction mechanism and the origin of the enantioselectivity.

Introduction

The increasing demand for organofluorine compounds in the discovery of new drugs, agrochemicals, and functional materials has aroused extensive interest in developing new synthetic methods to access structurally diverse fluorine-containing molecules.[1] In particular, monofluoromethyl (CH_2F)-containing chiral compounds are valuable, because the introduction of a CH_2F group as a bioisosteric substitute for methyl, hydroxymethyl and other functionalities can often result in profound changes in the chemical and biological properties of parent molecules (Scheme 1a).[2] Consequently, significant progress has been made in the selective synthesis of CH_2F-containing chiral molecules in the recent decade.[3] While much attention has been paid to the synthesis and application of CH_2F-tethered stereocenters, the construction of CH_2F-tethered axial chirality remains an unconquered challenge (Scheme 1b).[3a]

On the other hand, axial chirality represents a prominent structural motif in pharmaceuticals and bioactive natural products. Among them, chiral allenes are a particularly important type of axially chiral pharmacophore,[4] as well as versatile

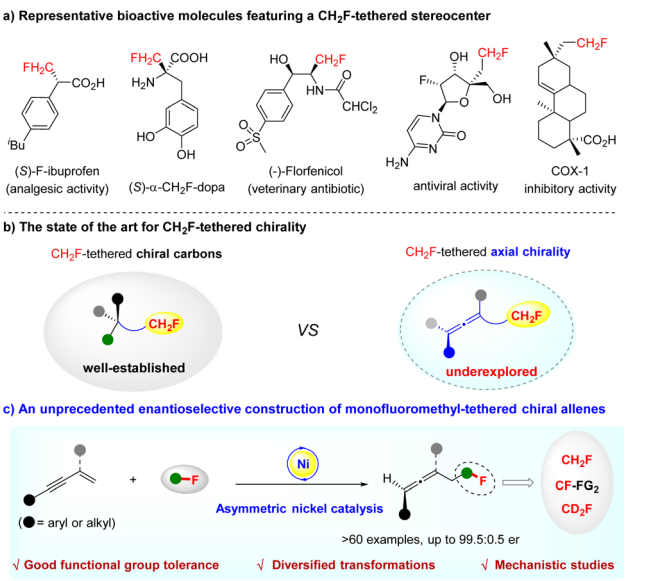

Scheme 1 The state of the art for CH_2F-tethered chirality and the current work.

[a]State Key Laboratory of Molecular & Process Engineering, Shanghai Engineering Research Center of Molecular Therapeutics and New Drug Development, School of Chemistry and Molecular Engineering, East China Normal University, Shanghai 200062, China. E-mail: jsyu@chem.ecnu.edu.cn

[b]Key Laboratory of Organofluorine Chemistry, Shanghai Institute of Organic Chemistry, Chinese Academy of Sciences, Shanghai 200032, China. E-mail: xuexs@sioc.ac.cn

[c]Hubei Key Laboratory of Quality Control of Characteristic Fruits and Vegetables, Hubei Engineering University, Xiaogan, 432000, China

[d]School of Chemistry and Materials Science, Hangzhou Institute for Advanced Study, University of Chinese Academy of Sciences, Hangzhou 310024, China

† Electronic supplementary information (ESI) available. CCDC 2275110, 2275115 and 2277305. For ESI and crystallographic data in CIF or other electronic format see DOI: https://doi.org/10.1039/d3sc04474b

‡ Y. Z., J. Y. and Y.-L. R. contributed equally to this work.

building blocks in organic synthesis.[5] The catalytic asymmetric synthesis of axially chiral allenes has accordingly attracted considerable attention over the past decade.[6] Despite great achievements, the enantioselective construction of optically active fluorine-containing allenes is still largely underdeveloped.[7] Therefore, the design and synthesis of diverse fluorinated chiral allenes, especially the challenging CH_2F- or CD_2F-tethered chiral allenes, represent a very important task.

Against this background, together with our research interest in selective fluoroalkylation of unsaturated hydrocarbons,[8] we envisioned whether it would be possible to realize the access of CH_2F-tethered chiral allenes *via* a regio- and enantio-selective hydromonofluoromethylation of 1,3-enynes[9] by asymmetric nickel catalysis[10] (Scheme 1c). Such research is, however, confronted with the following challenges: (i) the feasibility of a nickel catalyst to activate 1,3-enynes—nickel-catalysed hydrofunctionalization of 1,3-enynes has not yet been explored; (ii) not knowing how a nickel species initiates the reaction, and effects that control the enantioselectivity; (iii) the quest for a readily convertible fluoroalkylation reagent.

Herein, we successfully implemented this challenging transformation. We develop an unprecedented nickel-catalysed regio- and enantio-selective hydromonofluoromethylation of 1,3-enynes with fluorobis(phenylsulfonyl)methane (FBSM)[11] that proves to be a robust monofluoromethyl reagent for installing a CH_2F-tethered stereocenter.[3a,12] It provides a facile and efficient route to axially chiral allenes featuring a CH_2F or CD_2F moiety that cannot be accessed by known methods (Scheme 1c). Notably, this constitutes the first application of an earth-abundant and low-cost redox-neutral asymmetric nickel catalysis for enabling the asymmetric 1,4-hydrofunctionalization of 1,3-enynes.

Results and discussion

Optimization of the reaction conditions

We initiated this study by investigating different chiral ligands for the model reaction of but-3-en-1-yn-1-ylbenzene **1a** and FBSM **2a** in EtOH at room temperature (rt) under $Ni(COD)_2$ (10 mol%) catalysis, as shown in Table 1. *P*-Chiral ligand (*S*,*S*)-QuinoxP* (**L1**, 10 mol%) was first examined under base-free conditions; however, only a trace amount of the desired fluorine-containing allene **3a** was detected, accompanied by the remainder of both starting materials (entry 1). We then proceeded to add a base, to enable the reaction. To our delight, we found that upon the addition of Et_3N (1.0 equiv.) the reaction proceeded smoothly, affording allene **3a** in 48% yield with 94 : 6 er (entry 2). Encouraged by this positive result, we then explored the performance of other chiral bisphosphine ligands and *P*,*N*-based PHOX ligands in the presence of Et_3N (entries 3–9). The use of axially chiral (*R*)-MeO-BIPHEP (**L3**) greatly improved the reactivity and afforded **3a** in 68% yield with 94.5 : 5.5 er (entry 4). Subsequently, an investigation into the solvent effect revealed that almost no product was observed when using a non-protonic solvent such as toluene or THF (entries 10 and 11). EtOH remained the best solvent (entry 4), although the use of other alcoholic solvents could give a similar reaction outcome

Table 1 Selected conditions for optimization[a]

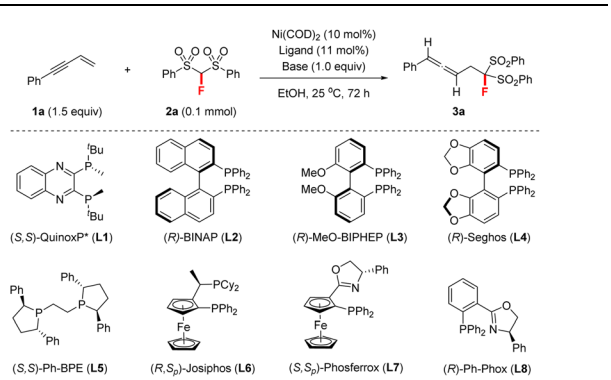

Entry	Ligand	Base	Solvent	Yield[b] (%)	er[c]
1	**L1**	—	EtOH	Trace	—
2	**L1**	Et_3N	EtOH	48	94 : 6
3	**L2**	Et_3N	EtOH	57	86 : 14
4	**L3**	Et_3N	EtOH	68	94.5 : 5.5
5	**L4**	Et_3N	EtOH	40	94 : 6
6	**L5**	Et_3N	EtOH	38	95 : 5
7	**L6**	Et_3N	EtOH	15	78 : 22
8	**L7**	Et_3N	EtOH	26	93 : 7
9	**L8**	Et_3N	EtOH	12	81 : 19
10	**L3**	Et_3N	Toluene	nr	—
11	**L3**	Et_3N	THF	nr	—
12	**L3**	Et_3N	MeOH	68	93.5 : 6.5
13	**L3**	Et_3N	^{i}PrOH	62	95.5 : 4.5
14	**L3**	DIPEA	EtOH	73	94.5 : 5.5
15	**L3**	DABCO	EtOH	93	96 : 4
16	**L3**	Quinuclidine	EtOH	21	95 : 5
17[d]	**L3**	DABCO	EtOH	81	95 : 5
18[e]	**L3**	DABCO	EtOH	52	95 : 5
19[f]	**L3**	DABCO	EtOH	49	96 : 4
20[g]	**L3**	DABCO	EtOH	16	95 : 5

[a] Conditions: **1a** (0.15 mmol), **2a** (0.10 mmol), $Ni(COD)_2$ (10 mol%), ligand (11 mol%), and base (1.0 equiv.), at 25 °C for 72 h in the indicated solvent (1.0 mL), unless otherwise noted. [b] Determined by ^{1}H NMR analysis of the crude product using 1,3,5-trimethoxybenzene as the internal standard. [c] Determined by chiral HPLC analysis. [d] DABCO (50 mol%). [e] DABCO (20 mol%). [f] $Ni(COD)_2$ (5 mol%) and **L3** (5.5 mol%) was used. [g] $Ni(COD)_2$ (1 mol%) and **L3** (1.1 mol%) was used.

(entries 12 and 13). Furthermore, organic bases, including DIPEA, DABCO, and quinuclidine, were investigated (entries 14–16). DABCO proved to be the optimal base in terms of reactivity and enantioselectivity (entry 15). Finally, we found that reducing the loading of DABCO or chiral nickel catalyst significantly decreased the yield of **3a**, albeit without loss of enantioselectivity (entries 17–20).

Evaluation of substrate scope

Having established the optimized reaction conditions, we then explored the scope of hydromonofluoromethylation between 1,3-enynes **1** and FBSM **2**. The effect of the substituents on the aromatic ring of 1,3-enynes **1** was evaluated (see Scheme 2). 1,3-Enynes with electron-withdrawing and electron-donating groups were all suitable substrates, affording the

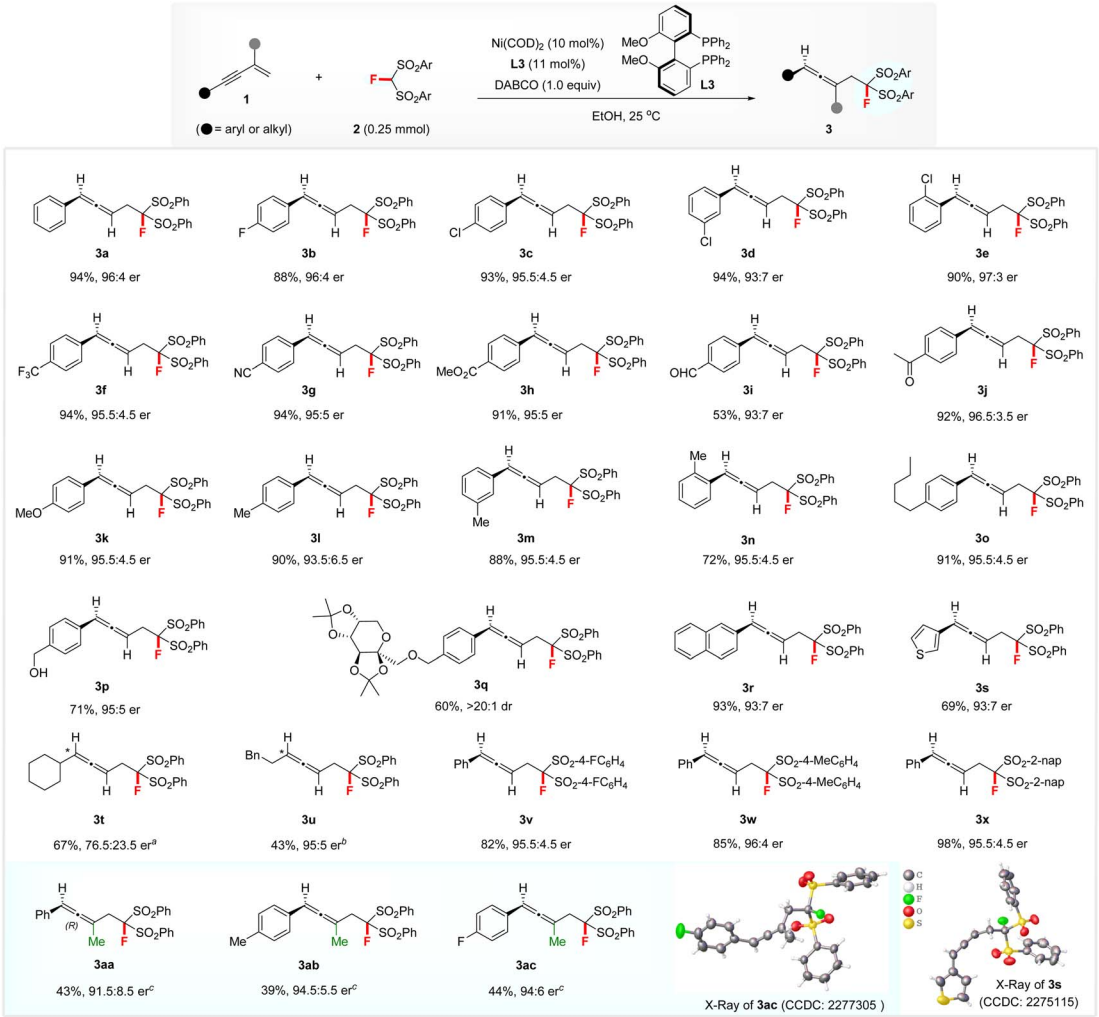

Scheme 2 Scope of hydromonofluoromethylation of 1,3-enynes **1** with FBSM **2**. Reaction conditions: **1** (0.375 mmol), **2** (0.25 mmol), $Ni(COD)_2$ (10 mol%), **L3** (11 mol%), and DABCO (1.0 equiv.), at 25 °C in EtOH (2.5 mL), unless otherwise noted. Yields of isolated products are reported. The er was determined by chiral HPLC analysis. [a](*S*)-Difluorphos (**L9**) was used instead of **L3**, at 40 °C. [b]Josiphos SL-J009-1 (**L10**) was used instead of **L3**, at 40 °C. [c](*S*,*S*)-BenzP* (**L11**) was used instead of **L3**, at 60 °C.

corresponding products **3b–3q** with up to 97 : 3 er. Notably, this transformation tolerated various functionalities on the phenyl ring of 1,3-enynes, such as halide (**3b–3e**), CF_3 (**3f**), cyano (**3g**), ester (**3h**), formyl (**3i**), acetyl (**3j**), hydroxymethyl (**3p**), and diacetone fructose (**3q**). Slightly lower enantiomeric ratios were obtained for 2-naphthyl- and 3-thienyl-substituted 1,3-enynes (**3r** and **3s**). The absolute configuration of **3s** was determined to be (*R*) by its X-ray diffraction (XRD) analysis. Subsequently, (*R*) was assigned to all other disubstituted allenes **3** by analogy. Aliphatic 1,3-enynes with a cyclohexyl or phenylethyl group also afforded the targets **3t** and **3u** with moderate to high enantioselectivities, when using (*S*)-difluorphos (**L9**) or Josiphos SL-J009-1 (**L10**) as the ligand. Additionally, differently substituted FBSM **2** materials were compatible with the reaction conditions, giving rise to products **3v–3x** in 82–98% yields with 95.5 : 4.5–96 : 4 er. Remarkably, 1,3-enynes featuring a methyl group at the 2-position were also tolerated.[13] The corresponding fluorine-containing trisubstituted allenes **3aa–3ac** were obtained with up to 94 : 6 er under the action of a 20 mol% (*S*,*S*)-BenzP* (**L11**) decorated chiral nickel catalyst at 60 °C. XRD analysis revealed that the absolute configuration of **3ac** was (*R*) and that of products **3aa** and **3ab** was assigned by analogy.

To illustrate the generality of this nickel-catalysed enantioselective hydrofluoromethylation process, we next investigated the reaction of 1,3-enynes **1** with diethyl fluoromalonate **4** for the construction of functionalized chiral allenes featuring a fluorine atom and two convertible ester groups[14] (Scheme 3). Gratifyingly, a variety of aryl 1,3-enynes **1** were amenable to the reaction under the above standard conditions, affording a variety of functionalized chiral allenes **5a–5u** in good to excellent yields with 95 : 5–98 : 2 er. The position and nature of the substituents on the aryl group have no obvious influence on enantioselectivity and reactivity. The diacetone fructose-derived aryl 1,3-enyne appeared to also be tolerated, affording the product **5q** in 94% yield with >20 : 1 dr. Both 2-naphthyl- and 1-naphthyl-substituted 1,3-enynes afforded the corresponding

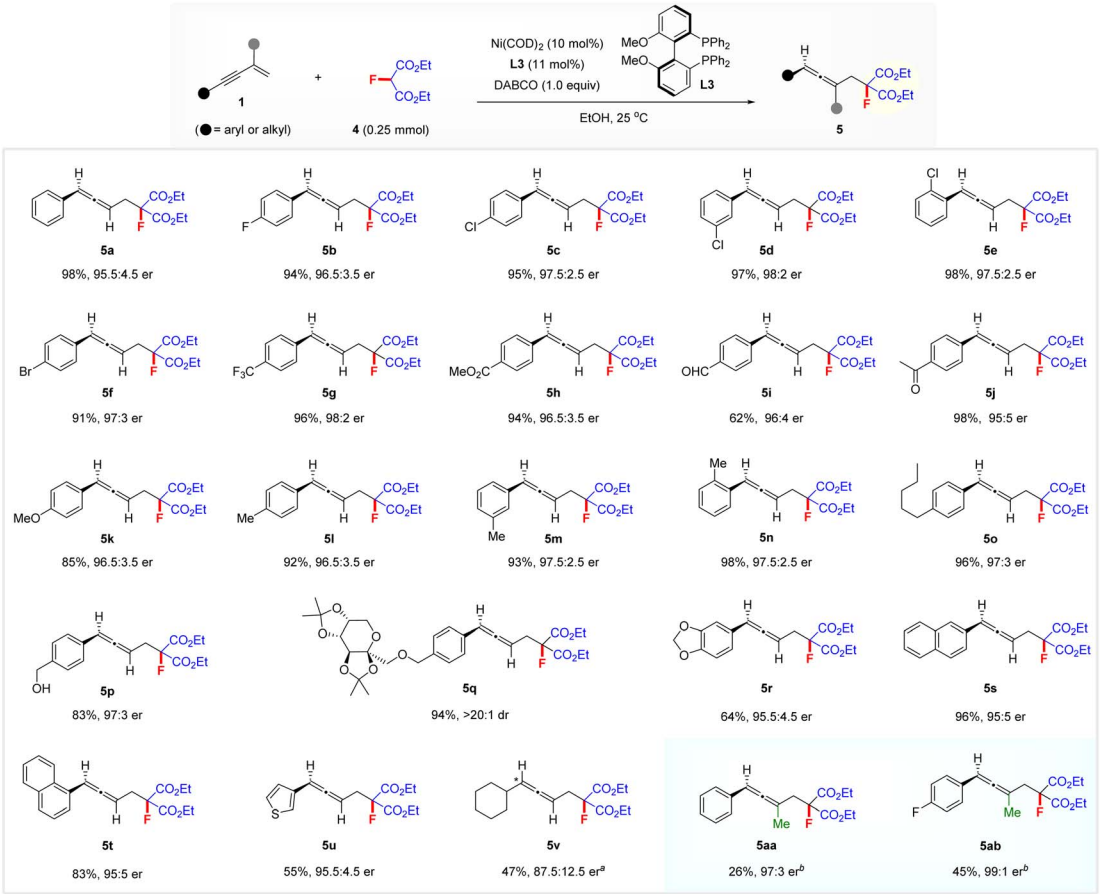

Scheme 3 Scope of hydromonofluoroalkylation of 1,3-enynes **1** with diethyl fluoromalonate **4**. Reaction conditions: **1** (0.375 mmol), **4** (0.25 mmol), $Ni(COD)_2$ (10 mol%), **L3** (11 mol%), and DABCO (1.0 equiv.), at 25 °C in EtOH (1.25 mL), unless otherwise noted. Yields of isolated products are reported. The er was determined by chiral HPLC analysis. [a]**L9** was used instead of **L3**, at 40 °C. [b]**L11** was used instead of **L3**, at 60 °C.

allenes **5s** in 96% yield with 95 : 5 er and **5t** in 83% yield with 95 : 5 er, respectively. Heteroaromatic 3-thienyl 1,3-enyne also delivered allene **5u** with 95.5 : 4.5 er. In addition, cyclohexyl-substituted aliphatic 1,3-enyne was a viable substrate under the optimized conditions, affording the 1,3-dialkyl allene **5v** with 87.5 : 12.5 er when employing **L9** instead of **L3** at elevated temperature. Notably, 2-methyl 1,3-enynes also reacted smoothly with **4** in the presence of 20 mol% (*S*,*S*)-BenzP* (**L11**)/$Ni(COD)_2$ at 60 °C, affording the functionalized trisubstituted allenes **5aa** with 97 : 3 er and **5ab** with 99 : 1 er.

Synthetic utility

The synthetic potential of this method was further highlighted by the direct synthesis of CH_2F-or CD_2F-tethered chiral allenes, gram-scale synthesis, and the diverse product transformations toward other fluorinated compounds, as depicted in Scheme 4. First, we directed our efforts toward the challenging CH_2F- or CD_2F-tethered chiral allenes by combining Ni-catalysed hydromonofluorobis(phenyl-sulfonyl)methylation with a sequential Mg-enabled reductive desulfonylation. Gratifyingly, treatment of the crude product of the hydrofluoroalkylation with Mg/MeOH smoothly afforded the desired CH_2F-tethered chiral allenes **6a–6e** with high to excellent enantioselectivity, while the corresponding CD_2F-tethered chiral allenes **D-6a–6e** were obtained with up to 95.5 : 4.5 er when using CD_3OD as the solvent in the desulfonylation step (Scheme 4a). Notably, the stereoselective installation of a CD_2F group into the stereocenter is still a challenging task and remains underexplored, while the development of efficient protocols toward deuterated molecules is of current interest.[15]

Furthermore, a large-scale reaction between **1a** (7.5 mmol) and **4** (5.0 mmol) proceeded smoothly by simply using 5 mol% of chiral Ni complex, affording 1.3 g of allene **5a** in 91% yield with 97 : 3 er. The product **5a** was rich in functionality and useful as a versatile synthon to access other fluorine-containing molecules (Scheme 4b). The two ester functionalities in **5a** were readily either reduced to form the chiral allene-tethered fluorinated diol **7** (89% yield and 96.5 : 3.5 er) or hydrolyzed to allene-substituted dicarboxylic acid **8** (95% yield). XRD analysis of diol **7** confirmed its absolute configuration to be (*R*), and thus the absolute configuration of the other allene products **5** could be assigned. Interestingly, allene diol **7** underwent a gold-catalysed cyclization *via* an axial-to-central chirality transfer process to deliver optically active fluorinated tetrahydrofuran **9** featuring 1,3-stereocenters—a key skeleton in many natural products and

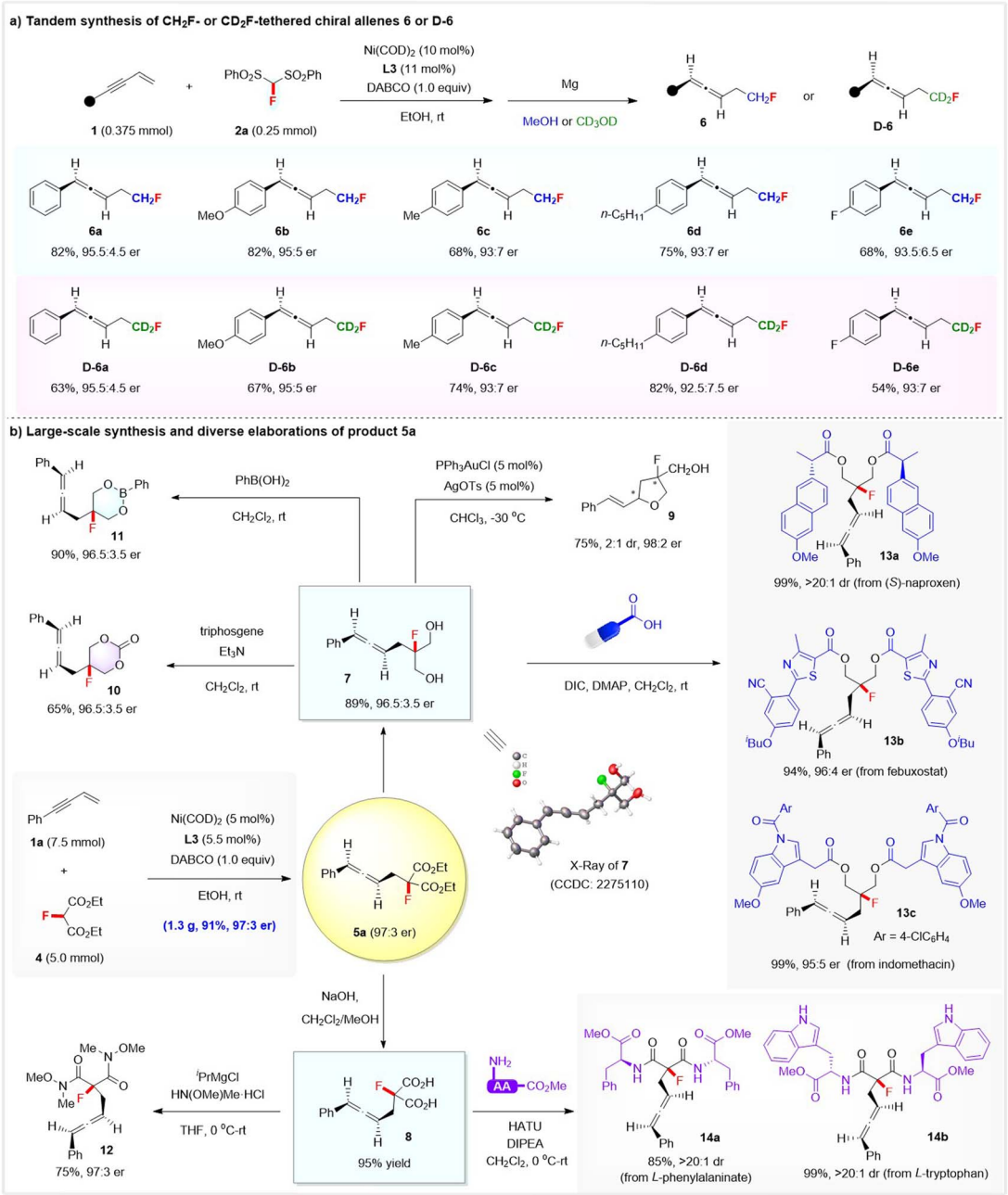

Scheme 4 Synthetic utility.

bioactive molecules such as the anti-HCV drug sofosbuvir. Chiral allene-containing fluorinated 1,3-dioxane-2-one **10** (65% yield and 96.5 : 3.5 er) or 1,3,2-dioxaborinane **11** (90% yield and 96.5 : 3.5 er) was readily obtained upon treatment of diol **7** with triphosgene or $PhB(OH)_2$, respectively. Dicarboxylic acid **8** reacted well with HN(OMe)Me·HCl to afford the corresponding allene Weinreb amide **12** in 75% with 97 : 3 er. Moreover, enantioenriched allene diol **7** and acid **8** proved to be very useful synthons in the late-stage modification of drugs and amino acids, as exemplified by the diverse assembly of chiral allene-containing drug derivatives **13a–13c** from (*S*)-naproxen, febuxostat, and indomethacin, as well as **14a–14b** from methyl L-tryptophanate or L-phenylalaninate.

Mechanistic studies

To gain insight into the reaction mechanism, we first conducted a deuterium-labeling experiment (Scheme 5a). When performing the reaction of **1a** and **2a** in ethanol-*d*1 (EtOD) under standard conditions, we found that the deuterium label is confined to C1 in **3a** (87% D-labeled); no deuterium incorporation was detected in the recovered enyne **1a** (eqn (1)). Under the above conditions using EtOD, there was also no H–D scrambling in

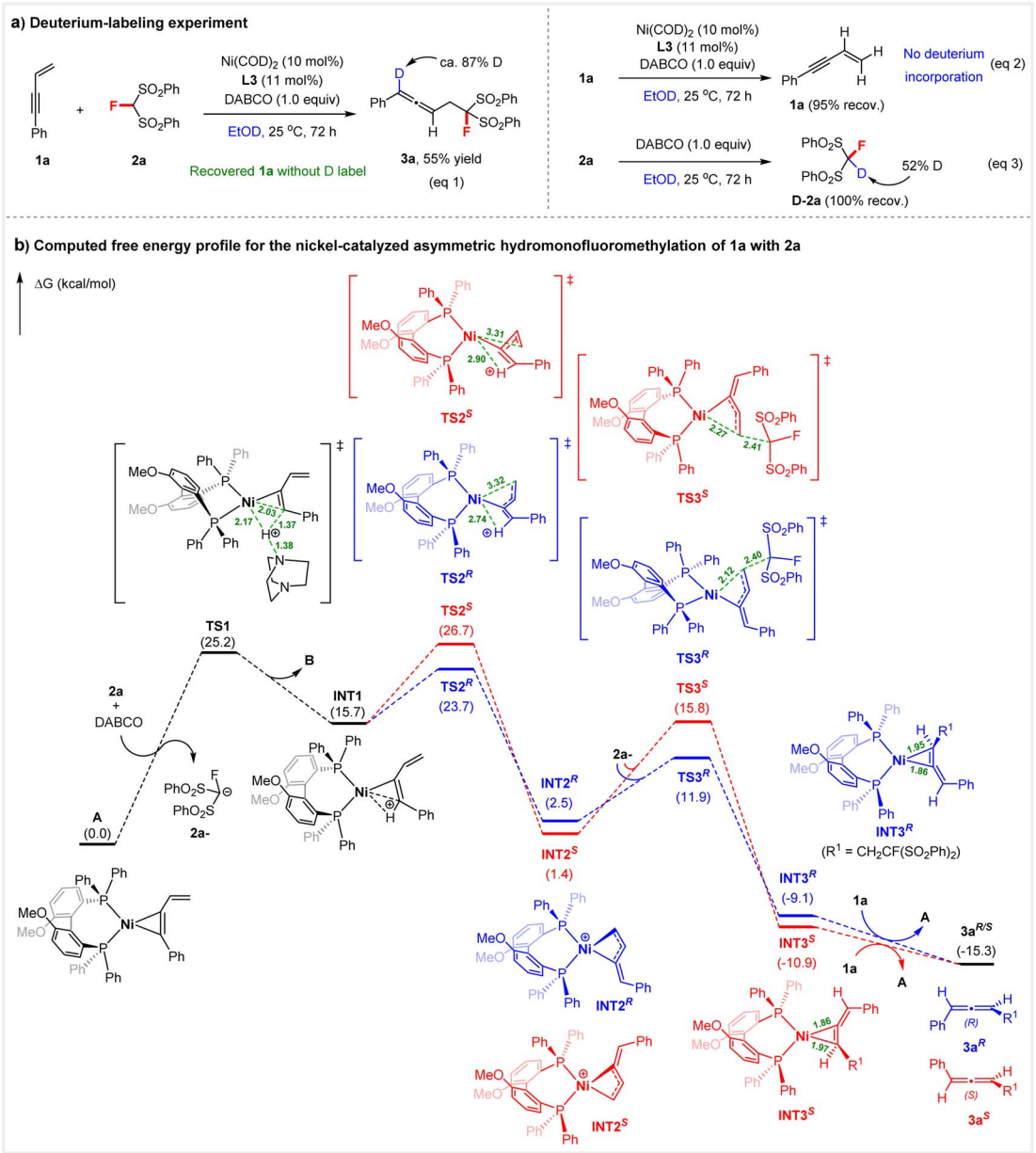

Scheme 5 Mechanistic investigation. Free energy profile and selected geometric parameters of key species (distances in angstrom) at the PBE0-D3(BJ)/def2-TZVP/PCM(EtOH)//PBE0-D3(BJ)/def2-SVP level.

enyne **1a** in the absence of **2a** (eqn (2)). We therefore concluded that insertion of the alkyne into the nickel hydride (Ni–H) occurs selectively, and the protonation of **1a** might not be accomplished by ethanol independently.

Meanwhile, DFT calculations at the PBE0-D3(BJ)[16a,b]/def2-TZVP[16c]/PCM(EtOH)[17]//PBE0-D3(BJ)/def2-SVP[16c] level were performed to gain a better understanding of the mechanism and the origin of the enantioselectivity of the hydromonofluoromethylation of **1a** with **2a** (Scheme 5b). The catalytic cycle commences with the protonation of active species **A** (see Fig. S4† for more details on the generation of **A** from $Ni(COD)_2$) by protonated DABCO ($\mathbf{BH^+}$), which is formed from DABCO (**B**) and **2a**, giving η^1-coordinated butadienyl–Ni complex **INT1**. This step needs to overcome a free energy barrier of 25.2 kcal mol^{-1}. The observed H–D exchange of **2a** with EtOD in the presence of DABCO supports the process (eqn (3), Scheme 5a).

On this basis, the mechanism for the generation of intermediate **INT1** *via* the activation of 1,3-enyne with the Ni complex is different from the traditional Pd–H species initiated enantioselective 1,3-enyne hydrofunctionalizations.[9b,h] Subsequently, isomerization of **INT1** by rotation of the protonated enyne ligand occurs *via* **TS2** to give a more stable η^3-butadienyl-Ni **INT2**, which is then attacked by the anion $\mathbf{2a^-}$ in an outer-sphere manner, to give the **3a** ligated complex **INT3**. Finally, ligand exchange between **1a** and **3a** takes place to complete the catalytic cycle. The enantioselectivity-determining step is the

isomerization of **INT1**, in which there are two directions for ligand rotation, corresponding to **TS2**^{S} and **TS2**^{R}, respectively. **TS2**^{S} is 3.0 kcal mol^{-1} less stable than **TS2**^{R} (26.7 kcal mol^{-1} *vs.* 23.7 kcal mol^{-1}). For the subsequent nucleophilic attack step, the *R*-conformation is more facile than the *S*-conformation (11.9 kcal mol^{-1} of **TS3**^{R} *vs.* 15.8 kcal mol^{-1} of **TS3**^{S}). These results are consistent with experimental observations.

To shed more light on the origin of enantioselectivity, energy decomposition analysis[18] towards **TS2**^{S} and **TS2**^{R} was carried out. In these transition states (TSs), the neutral Ni catalyst part is defined as fragment **F1** and the protonated enyne moiety as fragment **F2** (Scheme 6). The activation energy $\Delta E^{\ddagger}$ of the transition states can be written as $\Delta E^{\ddagger} = \Delta E_{\mathrm{def}} + \Delta E_{\mathrm{int}}$, where ΔE_{def} (deformation energy) is the energy difference that arises from structural changes toward the TS formation, and ΔE_{int} (interaction energy) corresponds to the energy difference between the two fragments (**F1** and **F2**) and the complex at the TS structure. The results indicate that although the interaction between the protonated enyne and Ni catalyst in **TS2**^{S} is stronger than that in **TS2**^{R} ($\Delta\Delta E_{\mathrm{int}} = -4.1$ kcal mol^{-1}), the deformation energy of **TS2**^{S} is much higher than that of **TS2R** by 7.1 kcal mol^{-1}, especially for the deformation of protonated enyne moiety **F2**, which governs the energy disparity between the two **TS**^{S}. Besides, the smaller C1–C2–C3 angle in **TS2**^{S} could also reflect the larger deformation of **F2** (Scheme 6b). It is likely due to the repulsion between the phenyl groups of the chiral ligand and vinyl group of **F2** with the nearest H···H distance of 2.29 Å in **TS2**^{S}, while in **TS2**^{R} the corresponding nearest H···H distance is significantly larger (2.46 Å). Such an effect could be the key factor causing the high enantioselectivity in this reaction.

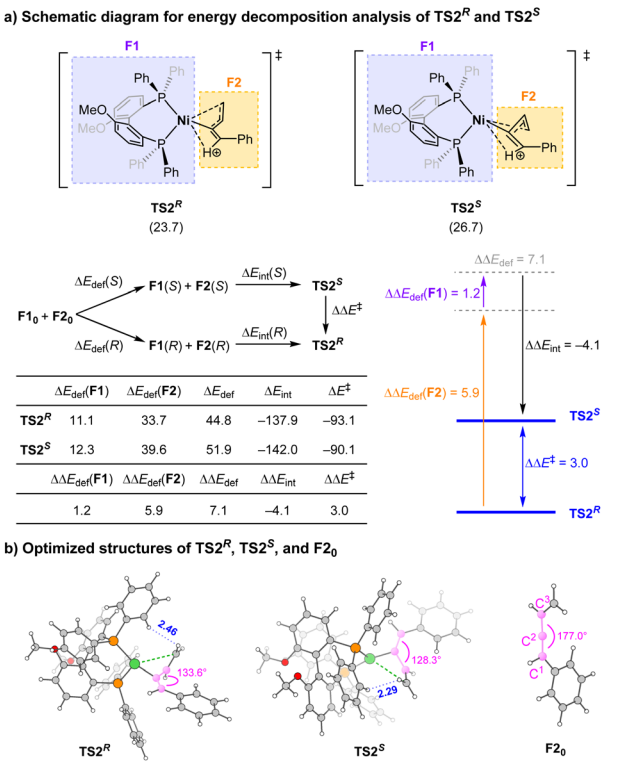

	ΔE_{def}(F1)	ΔE_{def}(F2)	ΔE_{def}	ΔE_{int}	$\Delta E^{\ddagger}$
TS2^{R}	11.1	33.7	44.8	−137.9	−93.1
TS2^{S}	12.3	39.6	51.9	−142.0	−90.1
	$\Delta\Delta E_{\mathrm{def}}$(F1)	$\Delta\Delta E_{\mathrm{def}}$(F2)	$\Delta\Delta E_{\mathrm{def}}$	$\Delta\Delta E_{\mathrm{int}}$	$\Delta\Delta E^{\ddagger}$
	1.2	5.9	7.1	−4.1	3.0

Scheme 6 Energy decomposition analysis. Energy decomposition analysis of **TS2**^{R} and **TS2**^{S} at the PBE0-D3(BJ)/def2-TZVP/PCM(EtOH) level, and $\Delta\Delta E_{\mathrm{def}}$(F1) = ΔE_{def}(F1-*S*) − ΔE_{def}(F1-*R*) (energies in kcal mol^{-1}); optimized structures and selected geometric parameters of **TS2**^{R}, **TS2**^{S}, and $\mathbf{F2}_0$ (distances in angstrom).

Conclusions

To summarize, we have established a regio- and enantio-selective hydromonofluoromethylation of 1,3-enynes with FBSM or diethyl fluoromalonate by redox-neutral asymmetric nickel catalysis, enabling us to access various monofluoromethylated chiral allenes, including the challenging CH_2F- or CD_2F-tethered ones. Moreover, the synthetic utility of this method is demonstrated by the following: the unprecedented preparation of CH_2F- or CD_2F-tethered chiral allenes, broad substrate scope, good functional group tolerance, and diverse product transformations to valuable functionalized fluorine-containing allenes or fluorinated tetrahydrofurans. The reaction mechanism and the origin of enantioselectivity were elucidated by DFT calculations and experimental studies. This also constitutes the first application of low-cost asymmetric nickel catalysis in activating 1,3-enynes for realizing asymmetric 1,4-hydrofunctionalizations, thus providing motivation for further developing enantioselective Ni-catalysed transformations of 1,3-enynes. The development of other regioselective hydrofluoroalkylation processes of 1,3-enynes by asymmetric nickel catalysis is currently ongoing in our laboratory.

Data availability

All of the experimental data have been included in the ESI.† Crystallographic data can be obtained from the CCDC (2277305, 2275110 and 2275115).

Author contributions

J.-S. Y. conceived the idea; Y. Z., Y.-L. R., L. L., and C. M. performed the experiments; J. Y. and X.-S. X. performed the DFT calculations; Y. Z. and Y.-L. R. collected and analyzed the data. J.-S. Y. and X.-S. X. directed the project and co-wrote the manuscript. All authors reviewed and edited the manuscript.

Conflicts of interest

There are no conflicts to declare.

Acknowledgements

This work was financially supported by the National Key Research and Development Program of China (2021YFC2102400), the National Natural Science Foundation of China (Grant No. 22171087 and 22122104, 22193012, and 21933004), the Shanghai Science and Technology Innovation Action Plan (21N41900500 and 20JC1416900), the Ministry of Education (PCSIRT) and the Fundamental Research Funds for the Central Universities. J.-S. Y. also acknowledges financial support from the "Zijiang Scholar

Program" of East China Normal University (ECNU). We acknowledge Prof. Dr Jian Zhou at ECNU for his valuable discussion.

Notes and references

1 (*a*) S. Purser, P. R. Moore, S. Swallow and V. Gouverneur, *Chem. Soc. Rev.*, 2018, **37**, 320–330; (*b*) J. Wang, M. Sánchez-Roselló, J. Aceña, C. del Pozo, A. E. Sorochinsky, S. Fustero, V. A. Soloshonok and H. Liu, *Chem. Rev.*, 2014, **114**, 2432–2506; (*c*) P. Kirsch, *Modern Fluoroorganic Chemistry: Synthesis Reactivity, Applications*, Wiley-VCH, Weinheim, 2nd edn, 2013.

2 (*a*) J. Kollonitsch, A. Patchett, S. Marburg, A. L. Maycock, L. M. Perkins, G. A. Doldouras, D. E. Duggan and S. D. Aster, *Nature*, 1978, **274**, 906–908; (*b*) H. Su, Y. Xie, W.-B. Liu and S.-L. You, *Bioorg. Med. Chem. Lett.*, 2011, **21**, 3578–3582. Also see a review:; (*c*) N. A. Meanwell, *J. Med. Chem.*, 2018, **61**, 5822–5880.

3 For leading reviews: (*a*) M. Reichel and K. Karaghiosoff, *Angew. Chem., Int. Ed.*, 2020, **59**, 12268–12281; (*b*) X. Yang, T. Wu, R. J. Phipps and F. D. Toste, *Chem. Rev.*, 2015, **115**, 826–870; (*c*) T. Furuya, A. S. Kamlet and T. Ritter, *Nature*, 2011, **473**, 470–477.

4 A. Hoffmann-Röder and N. Krause, *Angew. Chem., Int. Ed.*, 2004, **43**, 1196–1216.

5 (*a*) S. Ma, *Acc. Chem. Res.*, 2009, **42**, 1679–1688; (*b*) S. Yu and S. Ma, *Angew. Chem., Int. Ed.*, 2012, **51**, 3074–3112; (*c*) C. S. Adams, C. D. Weatherly, E. G. Burke and J. M. Schomaker, *Chem. Soc. Rev.*, 2013, **43**, 3136–3163.

6 (*a*) *Axially Chiral Compounds: Asymmetric Synthesis and Applications*, ed. B. Tan, Wiley-VCH GmbH, 2021, ch. 6, p. 141; (*b*) M. Ogasawara, *Tetrahedron: Asymmetry*, 2009, **20**, 259–271; (*c*) R. K. Neff and D. E. Frantz, *ACS Catal.*, 2019, **4**, 519–528; (*d*) W.-D. Chu, Y. Zhang and J. Wang, *Catal. Sci. Technol.*, 2017, **7**, 4570–4579; (*e*) W. Xiao and J. Wu, *Org. Chem. Front.*, 2022, **9**, 5053–5073; (*f*) Y. Li and H. Bao, *Chem. Sci.*, 2022, **13**, 8491–8506; (*g*) X. Wang, X. Chen, W. Lin, P.-F. Li and W.-J. Li, *Adv. Synth. Catal.*, 2022, **364**, 1212–1222.

7 Known examples for the construction of fluorinated chiral allenes: (*a*) T. J. O'Connor, B. K. Mai, J. Nafie, P. Liu and F. D. Toste, *J. Am. Chem. Soc.*, 2021, **143**, 13759–13768; (*b*) J. S. Ng and T. Hayashi, *Angew. Chem., Int. Ed.*, 2021, **60**, 20771–20775; (*c*) S.-Q. Yang, Y.-F. Wang, W.-C. Zhao, G.-Q. Lin and Z.-T. He, *J. Am. Chem. Soc.*, 2021, **143**, 7285–7291; (*d*) Y. Zeng, M.-F. Chiou, X. Zhang and H. Bao, *J. Am. Chem. Soc.*, 2020, **142**, 18014–18021; (*e*) J. Dai, X. Duan, J. Zhou, C. Fu and S. Ma, *Chin. J. Chem.*, 2018, **36**, 387–391.

8 (*a*) J.-S. Yu, F.-M. Liao, W.-M. Gao, K. Liao, R.-L. Zuo and J. Zhou, *Angew. Chem., Int. Ed.*, 2015, **54**, 7381–7385; (*b*) X.-S. Hu, J.-X. He, S.-Z. Dong, Q.-H. Zhao, J.-S. Yu and J. Zhou, *Nat. Commun.*, 2020, **11**, 5500; (*c*) L. Liao, Y. Zhang, Z.-W. Wu, Z.-T. Ye, X.-X. Zhang, G. Chen and J.-S. Yu, *Chem. Sci.*, 2022, **13**, 12519–12526; (*d*) X.-S. Hu, J.-X. He, Y. Zhang, J. Zhou and J.-S. Yu, *Chin. J. Chem.*, 2021, **39**, 2227–2233; (*e*) W.-B. Wu, B.-S. Mu, J.-S. Yu and J. Zhou, *Chem. Sci.*, 2022, **13**, 3519–3525.

9 For typical examples on the asymmetric functionalization of 1,3-enynes: (*a*) J.-W. Han, N. Tokunaga and T. Hayashi, *J. Am. Chem. Soc.*, 2001, **123**, 12915–12916; (*b*) N. J. Adamson, H. Jeddi and S. J. Malcolmson, *J. Am. Chem. Soc.*, 2019, **141**, 8574–8583; (*c*) L. Li, S. Wang, P. Luo, R. Wang, Z. Wang, X. Li, Y. Deng, F. Peng and Z.-D. Shao, *Nat. Commun.*, 2021, **12**, 5667; (*d*) Q. He, L. Zhu, Q. Ouyang, W. Du and Y.-C. Chen, *J. Am. Chem. Soc.*, 2021, **143**, 17989–17994; (*e*) Y. Huang, J. del Pozo, S. Torker and A. H. Hoveyda, *J. Am. Chem. Soc.*, 2018, **140**, 2643–2655; (*f*) L. Bayeh-Romero and S. L. Buchwald, *J. Am. Chem. Soc.*, 2019, **141**, 13788–13794; (*g*) Q. Li, X. Fang, R. Pan, H. Yao and A.-J. Lin, *J. Am. Chem. Soc.*, 2022, **144**, 11364–11376. Also see ref. 7c. For the related reviews:; (*h*) L. Li, S. Wang, A. Jakhar and Z. Shao, *Green Synth. Catal.*, 2023, **4**, 124–134; (*i*) L. Fu, S. Greßies, P. Chen and G.-S. Liu, *Chin. J. Chem.*, 2020, **38**, 91–100.

10 (*a*) C. L. Drennan, *Nat. Chem.*, 2010, **2**, 900; (*b*) Y. Wang, Y. He and S. Zhu, *Acc. Chem. Res.*, 2022, **55**, 3519–3536.

11 For the seminal work regarding FBSM: (*a*) T. Fukuzumi, N. Shibata, M. Sugiura, H. Yasui, S. Nakamura and T. Toru, *Angew. Chem., Int. Ed.*, 2006, **45**, 4973–4977; (*b*) C. Ni, Y. Li and J. Hu, *J. Org. Chem.*, 2006, **71**, 6829–6833.

12 For a review: (*a*) A.-N. R. Alba, X. Companyo and R. Rios, *Chem. Soc. Rev.*, 2010, **39**, 2018–2033. For selected examples, see: (*b*) S. Mizuta, N. Shibata, Y. Goto, T. Furukawa, S. Nakamura and T. Toru, *J. Am. Chem. Soc.*, 2007, **129**, 6394–6395; (*c*) T. Furukawa, N. Shibata, S. Mizuta, S. Nakamura, T. Toru and M. Shiro, *Angew. Chem., Int. Ed.*, 2008, **47**, 8051–8054; (*d*) T. Furukawa, J. Kawazoe, W. Zhang, T. Nishimine, E. Tokunaga, T. Matsumoto, M. Shiro and N. Shibata, *Angew. Chem., Int. Ed.*, 2011, **50**, 9684–9688; (*e*) H. Zheng, Z. Li, J. Jing, X.-S. Xue and J.-P. Cheng, *Angew. Chem., Int. Ed.*, 2021, **60**, 9401–9406.

13 We thank one referee for suggesting the examination of the result for 1-substituted 1,3-enynes. It was found that no desired product was observed when subjecting pent-3-en-1-yn-1-ylbenzene to the reaction with FBSM **2a** under the standard conditions, accompanied by the recovery of **2a** with >95%.

14 P. Xu and Z. Huang, *Nat. Chem.*, 2021, **13**, 634–642.

15 (*a*) C. Schmidt, *Nat. Biotechnol.*, 2017, **35**, 493–494; (*b*) V. Jacques, A. W. Czarnik, T. M. Judge, L. H. T. Van der Ploeg and S. H. DeWitt, *Proc. Natl. Acad. Sci. U. S. A.*, 2015, **112**, E1471–E1479.

16 (*a*) C. Adamo and V. Barone, *J. Chem. Phys.*, 1999, **110**, 6158–6170; (*b*) S. Grimme, J. Antony, S. Ehrlich and H. Krieg, *J. Chem. Phys.*, 2010, **132**, 154104; (*c*) F. Weigend and R. Ahlrichs, *Phys. Chem. Chem. Phys.*, 2005, **7**, 3297–3305.

17 (*a*) S. Miertuš, E. Scrocco and J. Tomasi, *Chem. Phys.*, 1981, **55**, 117–129; (*b*) B. Mennucci, E. Cancès and J. Tomasi, *J. Phys. Chem. B*, 1997, **101**, 10506–10517; (*c*) J. Tomasi, B. Mennucci and R. Cammi, *Chem. Rev.*, 2005, **105**, 2999–3094.

18 F. M. Bickelhaupt and K. N. Houk, *Angew. Chem., Int. Ed.*, 2017, **56**, 10070–10086.